https://doi.org/10.5194/ms-2026-196
Preprint. Discussion started: 19 November 2026
© Author(s) 2026. CC BY 4.0 License.



mechanical sciences
DISCUSSIONS

Chassis integrated control of intelligent vehicle based on adaptive GA-QP algorithm

Bin Tang, Yanjie Zhu, Haobin Jiang, Wei Mi

Automotive Engineering Research Institute, Jiangsu University, Jiangsu, China

Correspondence to: Bin Tang (tangbin@ujs.edu.cn)

Abstract. In order to improve the yaw stability of intelligent vehicle, the chassis integrated control strategy based on adaptive genetic-quadratic programming (GA-QP) algorithm is proposed in this paper. The hierarchical control architecture is adopted, the upper layer is a chassis integrated controller based on sliding mode control, which determines the lateral force, longitudinal force, and yaw moment. The lower layer is the tire force distribution strategy based on GA-QP algorithm. Furthermore, the parameters in the objective function of the GA-QP algorithm are adaptively adjusted based on the phase plane stability-judged principle to achieve the optimal distribution of each tire force. According to simulation results, the adaptive integrated control strategy reduces the side slip angle by 0.791 deg compared with unintegrated control strategy under cornering condition with high adhesion coefficient. Under low adhesion coefficient conditions, the side slip angle is reduced by 0.393 deg. In addition, the adaptive integrated control strategy distributes more longitudinal torque to the rear wheels, which avoids front tire force saturation. Consequently, the results demonstrate that the adaptive integrated control strategy proposed in this study effectively enhances the driving safety and handling stability of the vehicle.
Key words: Chassis integrated control, Vehicle stability, Adaptive GA-QP algorithm, Phase plane, Tire force distribution strategy

1 Introduction

With the development of intelligent vehicle technology, chassis integrated control is increasingly playing an important role in motion control of intelligent vehicle (Cheng et al., 2023). The chassis integrated control system combines sophisticated controllers, sensors, and actuators with optimal algorithms and control strategies to realize advanced functions such as real-time monitoring and intelligent regulation of vehicle status. However, the current chassis integrated control technology still faces some challenges, especially in the coordination or integration of the longitudinal and lateral control of the chassis which has become a key concern for scholars (Zhu et al., 2024).

Chassis control methods are generally divided into two main types: coordinated control and integrated control (Liu et al., 2023; Liu et al., 2021; Atindana et al., 2024; Tang and Khajepour, 2020; Li et al., 2024; Liang et al., 2021; Elhefnawy et al., 2020; Chen et al., 2024). In the field of coordinated control, Wu et al. (2022) proposed an intervention criterion of stability control for active front steering control (AFS) and direct yaw moment control (DYC), and designed the corresponding hierarchical control algorithm and yaw moment distribution strategy. Zhang et al. (2022) proposed a coordinated control method for active front steering (AFS) and anti-lock braking systems (ABS) based on distributed model predictive control (DMPC) integrating multi-agent theory to enhance braking safety and handling stability. Elhefnawy et al. (2021) developed an optimized coordinated control system for DYC and AFS based on fuzzy control, and the controller parameters are optimized through genetic algorithm. Lin et al. (2023) proposed a hierarchical coordinated control strategy based on AFS and DYC and used the phase plane method to provide an assessment basis for the safety of vehicle, so as to improve the stability of distributed drive electric buses. However, the coordinated control approach not only makes the control system more complicated but also requires the compatibility between the coordinated controller and each subsystem controller. In terms of the integrated control, Liu et al. (2022) proposed an integrated control architecture for AFS and DYC in distributed driven electric vehicles (DDEVs), which involves an online risk assessment and prediction model to solve a multi-objective, multi-constraint optimization problem based on robust sliding mode predictive control (SMPC). Xiao et al. (2022) proposed an integrated AFS, active suspension systems (ASS) and DYC control framework based on model predictive control (MPC)

https://doi.org/10.5194/ms-2026-196
Preprint. Discussion started: 19 November 2026
© Author(s) 2026. CC BY 4.0 License.



mechanical sciences
DISCUSSIONS

to obtain the longitudinal force, lateral force, and yaw moment. Zhao et al. (2019) proposed a multi-objective optimization method for chassis integrated system based on adaptive weighted particle swarm optimization algorithm to improve the optimization efficiency. Scholtz et al. (2024) developed an integrated controller for active rear steering (ARS) and rear differential braking (RDB) to improve lateral stability of off-road vehicles. The integrated control approach optimizes the output of each subsystem and allows each subsystem to exploit individual strengths, thereby improving the overall performance and reliability of the vehicle. However, existing researches predominantly focus on vehicle stability and lateral-longitudinal conflict control, often neglecting a comprehensive analysis of the relationship between longitudinal force and lateral force on the front and rear wheels under extreme conditions, which leads to unreasonable tire force distribution. The phase plane (Zhu et al., 2023) is usually used to assess system stability and convergence, therefore, this paper adopts the phase plane stability analysis method to adaptively distribute the longitudinal force and lateral force of the front and rear wheels, thereby enhancing vehicle stability and preventing tire force saturation.

The tire force distribution strategy for chassis integrated control is primarily developed based on the optimization theory (Choi and Moon, 2024; Vošahlík and Haniš, 2023; Chen et al., 2019; Song et al., 2019). Wang et al. (2022) proposed a path tracking control strategy for four-wheel independently driven electric vehicles, in which the upper controller obtains the desired yaw rate through the backstepping method, the optimal front wheel steering angle and external yaw moment are calculated based on the model predictive control algorithm in the lower controller and the external yaw moment was distributed to each tire according to the optimal allocation method. Jiang et al. (2022) designed a path-tracking controller for a six-wheel independently driven unmanned ground vehicle (6WID UGV) which employs a seeker optimization algorithm (SOA) for torque distribution to achieve the required yaw moment and longitudinal force while minimizing energy consumption during path tracking. The integrated control of trajectory tracking and yaw stability for autonomous vehicles was studied by Li et al. (2024). To optimize the distribution of longitudinal tire force (Li et al., 2024), a sliding mode control algorithm was utilized to generate an additional yaw moment, while a PID control algorithm was applied to realize accurate longitudinal speed tracking. In the most of existing studies, the quadratic programming method is employed to solve the tire forces. Nevertheless, the algorithm may converge to a local optimal solution if the initial point is not chosen correctly (Pérez-Villeda et al., 2020). To address the problem, the genetic-quadratic programming algorithm is employed in this paper to achieve more accurate tire force calculations.

The chassis integrated control strategy of intelligent vehicle based on the adaptive GA-QP algorithm is proposed in this paper to address the problem of improper tire force distribution in chassis integration control. In order to achieve properly tire force distribution, the GA-QP optimization algorithm is developed to effectively seek the global initial solution of tire force in a broad search space and then obtain the optimal solution in the local area. Moreover, the longitudinal force distribution parameters of front and rear wheels in the objective function of GA-QP algorithm are adjusted based on the phase plane stability-judged principle, so as to improve the vehicle's driving safety and maneuverability.

2 Chassis integrated control strategy

The developed chassis integrated control framework based on the adaptive GA-QP algorithm is illustrated in Figure 1. According to the front wheel angle and vehicle speed obtained by intelligent vehicle trajectory tracking, the reference model outputs the desired longitudinal speed, lateral speed and yaw rate. The sliding mode controller determines the desired longitudinal force, lateral force and yaw moment of the vehicle according to the desired longitudinal speed, lateral speed, and yaw rate. Under the constraints of the desired longitudinal force, lateral force and yaw moment, the tire force of each wheel is calculated by the GA-QP algorithm, and the distribution parameters in the GA-QP objective function are adjusted based on the phase plane stability-judged principle. The Dugoff tire inverse model and torque calculation function are used to determine the front wheel angle and driving torque or braking torque of each wheel.

https://doi.org/10.5194/ms-2026-196
Preprint. Discussion started: 19 November 2026
© Author(s) 2026. CC BY 4.0 License.



mechanical sciences DISCUSSIONS

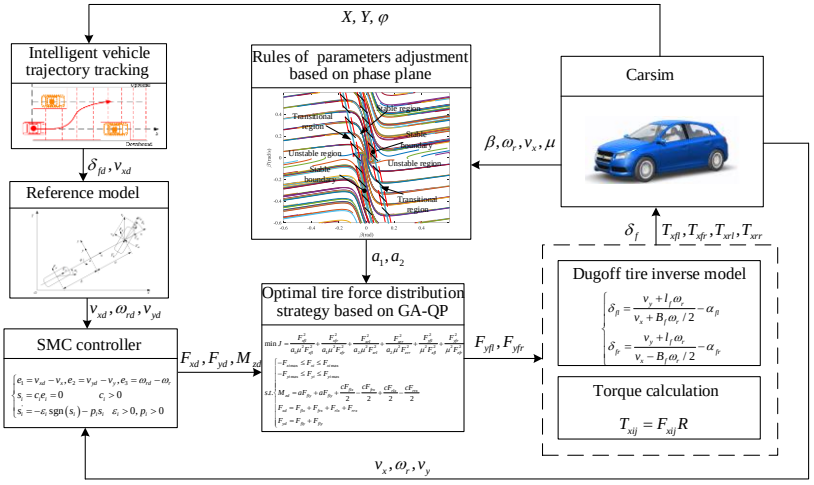


Figure 1. Chassis integrated control framework based on adaptive GA-QP algorithm.

2.1 Integrated controller design based on sliding mode control

Sliding mode control (SMC) is utilized extensively in various control fields due to its robustness, fast response and simple implementation. SMC is constructed in this paper based on three-degree-of-freedom model as shown in Figure 2. The differences between the desired longitudinal speed, lateral speed and yaw rate and their actual value are used as the sliding mode surface of SMC. The chassis integrated controller outputs the desired longitudinal force, lateral force and yaw moment of the vehicle.

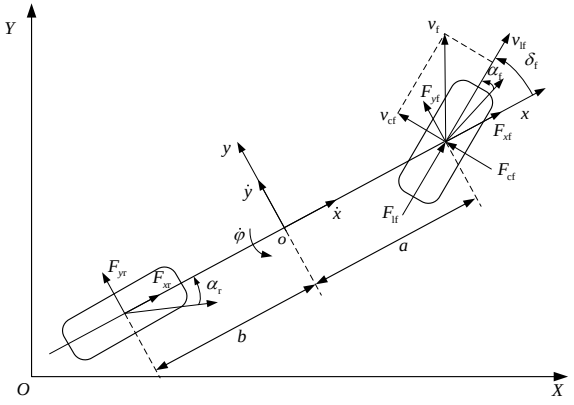


Figure 2. Three-degree-of-freedom dynamics model of the vehicle.

The dynamics equations of the vehicle are shown in Eq. (1).

$$\begin{cases} v_x^{'} = \dfrac{F_{xd}}{m} + v_y \omega_r \\ v_y^{'} = \dfrac{F_{yd}}{m} + v_x \omega_r \\ \omega_r^{'} = \dfrac{M_{zd}}{I_z} \end{cases} \tag{1}$$

https://doi.org/10.5194/ms-2026-196
Preprint. Discussion started: 19 November 2026
© Author(s) 2026. CC BY 4.0 License.



mechanical sciences DISCUSSIONS

where F_{xd} is longitudinal force of the vehicle, F_{yd} is lateral force of the vehicle, M_{zd} is the yaw moment, v_y and v_x represent the lateral and longitudinal speeds, respectively, m is the vehicle mass, ω_r denotes the yaw rate of the vehicle, I_z is the inertia of the vehicle around axis z, the state variable is $x_i = \begin{bmatrix} v_x & v_y & \omega_r \end{bmatrix}$, and the control variable is $u_i = \begin{bmatrix} F_{xd} & F_{yd} & M_{zd} \end{bmatrix}$.

The sliding mode surface and exponential convergence law of the sliding mode controller are presented as follows.

$$\begin{aligned} &e_1 = v_{xd} - v_x, e_2 = v_{yd} - v_y, e_3 = \omega_{rd} - \omega_r \\ &s_i = c_i e_i = 0 \qquad c_i > 0 \\ &\dot{s_i} = -\varepsilon_i \operatorname{sgn}(s_i) - p_i s_i \quad \varepsilon_i > 0, p_i > 0 \end{aligned} \tag{2}$$

where ω_{rd} denotes the desired yaw rate, $\omega_{rd} = \dfrac{1}{1+Kv_x^2}\dfrac{v_x}{L}\delta_f$, $|\omega_{rd}| \le \dfrac{0.85\mu g}{v_x}$, v_{yd} is the desired lateral speed, $v_{yd} = 0$, $c_i\,(i = 1,2,3)$ is the sliding mode control parameter, $c_i > 0$, ε_i, p_i are the exponential convergence law control parameters respectively, v_{xd} is the desired longitudinal speed, L denotes the distance from front axle to rear axle, δ_f is the front wheel angle, g is the gravitational acceleration, μ represents the adhesion coefficient.

To further eliminate the high frequency oscillation of the control output, a saturation function is introduced into the control law as follows.

$$sat\frac{s_i}{\Phi_i} = \begin{cases} \operatorname{sgn}(s_i) & |s_i| \ge \Phi_i \\ \dfrac{s_i}{\Phi_i} & |s_i| < \Phi_i \end{cases} \tag{3}$$

where Φ_i represents the boundary of sliding mode surface and $\Phi_i > 0$.

The control law is deduced from the above equations shown as follows.

$$\begin{aligned} F_{xd} &= \frac{m}{c_1}\left(c_1\left(\dot{v_{xd}} - v_y\omega_r\right) + \varepsilon_1 sat\frac{s_1}{\Phi_1} + p_1 s_1 \right) \\ F_{yd} &= \frac{m}{c_2}\left(c_2\left(\dot{v_{yd}} - v_x\omega_r\right) + \varepsilon_2 sat\frac{s_2}{\Phi_2} + p_2 s_2 \right) \\ M_{zd} &= \frac{I_z}{c_3}\left(c_3\dot{\omega_{rd}} + \varepsilon_3 sat\frac{s_3}{\Phi_3} + p_3 s_3 \right) \end{aligned} \tag{4}$$

The stability of the control system is assessed using the Lyapunov function, which must meet the following relationship.

$$\begin{cases} \lim\limits_{|s_i|\to\infty} V_i = \infty \\ \dot{V_i} < 0 \quad s_i \ne 0 \end{cases} \tag{5}$$

According to the Lyapunov theory, the following formula is obtained.

$$V_i = \frac{1}{2}s_i^2 \tag{6}$$

The derivative of V_i is calculated as follows.

$$\dot{V_i} = s_i\dot{s_i} = s_i\left(-\varepsilon_i \operatorname{sgn}(s_i) - p_i s_i\right) \le 0 \tag{7}$$

It is obvious that Eq. (7) satisfies the condition of the Lyapunov stability.

2.2 Tire force distribution based on GA-QP optimization algorithm

https://doi.org/10.5194/ms-2026-196
Preprint. Discussion started: 19 November 2026
© Author(s) 2026. CC BY 4.0 License.



mechanical sciences DISCUSSIONS

2.2.1 Objective function

In vehicle dynamics control, tire load rate is a crucial indicator to represent tire force utilization. An excessively high tire load rate causes the adhesion limitation of the tire, which worsens the safety margin of vehicle. By the optimization of tire force distribution, the load rate of each wheel tends to equilibrium state and the overall load rate is minimized, which can effectively prevent a single tire from reaching the adhesion limit prematurely and improve the stability and controllability of the vehicle. Therefore, the objective function of GA-QP optimization algorithm shown below is designed to optimize the average load rate of each wheel, so as to reduce the overall load rate of the vehicle and improve the handling stability.

$$\min J = \frac{F_{xfl}^2}{a_1\mu^2F_{zfl}^2} + \frac{F_{xfr}^2}{a_1\mu^2F_{zfr}^2} + \frac{F_{xrl}^2}{a_2\mu^2F_{zrl}^2} + \frac{F_{xrr}^2}{a_2\mu^2F_{zrr}^2} + \frac{F_{yfl}^2}{\mu^2F_{zfl}^2} + \frac{F_{yfr}^2}{\mu^2F_{zfr}^2} \tag{8}$$

where $F_{xij}\left(i=f,r;j=l,r\right)$ is the longitudinal force of each wheel, F_{yij} is the lateral force of each wheel, F_{zij} is the vertical force of each wheel, a_1, a_2 represent the front and rear longitudinal force distribution parameters, respectively.

The vertical force of each wheel is determined as follows.

$$\begin{cases} F_{zfl} = \dfrac{mgb}{2(a+b)} + \dfrac{ma_xh}{2\left(a+b\right)} + \dfrac{ma_yha}{B(a+b)} \\ F_{zfr} = \dfrac{mgb}{2(a+b)} + \dfrac{ma_xh}{2\left(a+b\right)} - \dfrac{ma_yha}{B(a+b)} \\ F_{zrl} = \dfrac{mga}{2(a+b)} - \dfrac{ma_xh}{2\left(a+b\right)} + \dfrac{ma_yhb}{B(a+b)} \\ F_{zrr} = \dfrac{mga}{2(a+b)} - \dfrac{ma_xh}{2\left(a+b\right)} - \dfrac{ma_yhb}{B(a+b)} \end{cases} \tag{9}$$

where a and b represent distance from the front axle to the center of mass and the rear axle to the center of mass respectively, a_x is the longitudinal acceleration of the vehicle, a_y is the lateral acceleration of the vehicle, h is the centroid height of vehicle, B is the front and rear track widths.

2.2.2 Constraint condition

In order to ensure that the lateral and longitudinal force of each wheel do not exceed the adhesion limit determined by the vertical load of each wheel and the road adhesion coefficient, constraint conditions of the optimization algorithm are established as follows.

$$\begin{cases} -F_{xij\max} \le F_{xij} \le F_{xij\max} \\ -F_{yij\max} \le F_{yij} \le F_{yij\max} \end{cases} \tag{10}$$

where $F_{xij\max}$ is the maximum longitudinal force of each wheel, $F_{yij\max}$ is the maximum lateral force of each wheel.

The following equality constraints are established for the optimization of longitudinal and lateral tire force based on the desired longitudinal force, lateral force and yaw moment.

$$\begin{cases} M_{zd} = aF_{yfl} + aF_{yfr} + \dfrac{BF_{xfl}}{2} - \dfrac{BF_{xfr}}{2} + \dfrac{BF_{xrl}}{2} - \dfrac{BF_{xrr}}{2} \\ F_{xd} = F_{xfl} + F_{xfr} + F_{xrl} + F_{xrr} \\ F_{yd} = F_{yfl} + F_{yfr} \end{cases} \tag{11}$$

https://doi.org/10.5194/ms-2026-196
Preprint. Discussion started: 19 November 2026
© Author(s) 2026. CC BY 4.0 License.



mechanical sciences DISCUSSIONS

2.2.3 Optimization solution

The genetic algorithm (GA) (Yang et al., 2021) has strong global search capability but weak local search capability, whereas the quadratic programming (QP) algorithm is good at local optimization. With the advantages of both methods be considered, the GA-QP optimization algorithm is developed which adopts the iterative results of genetic algorithm as the initial value of quadratic programming algorithm. The optimization process of the GA-QP algorithm is illustrated in Figure 3.

The mathematical model of the genetic algorithm is shown as follows.

$$GA=\begin{bmatrix} P & M & V & F & S_e & P_c & P_m & T \end{bmatrix} \tag{12}$$

where P is the initial population, M is population size, $M=50$, V is number of variables, $V=6$, S_e is the selection operator, $S_e=0.5$, P_c is the crossover operator probability, $P_c=0.8$, P_m is the mutation operator probability, $P_m=0.3$, T is the number of iterations, $T=100$, F is the fitness function, $F=-\left(\frac{F_{xfl}^2}{a_1\mu^2F_{zfl}^2}+\frac{F_{xfr}^2}{a_1\mu^2F_{zfr}^2}+\frac{F_{xrl}^2}{a_2\mu^2F_{zrl}^2}+\frac{F_{xrr}^2}{a_2\mu^2F_{zrr}^2}+\frac{F_{yfl}^2}{\mu^2F_{zfl}^2}+\frac{F_{yfr}^2}{\mu^2F_{zfr}^2}\right)$.

The steps of the GA-QP optimization algorithm are as follows:

Step1. Randomly generate a set of initial populations and calculate the fitness of each individual,
Step2. Select individuals into the next generation with a certain probability based on the fitness,
Step3. Perform crossover operations according to crossover probability,
Step4. Perform mutation operations according to mutation probability,
Step5. Judge whether the individual satisfies the constraint and fitness function, if so, output the search result, otherwise return to step 2,
Step6. Output the individual with the best fitness in the population as the optimal solution,
Step7. Use the output of genetic algorithm as initial solution of the quadratic programming,
Step8. Solve the tire force of each wheel based on the quadratic programming algorithm, the objective function of the quadratic programming algorithm is shown in Eq. (8), and the constraint conditions are shown in Eq. (10) and Eq. (11).

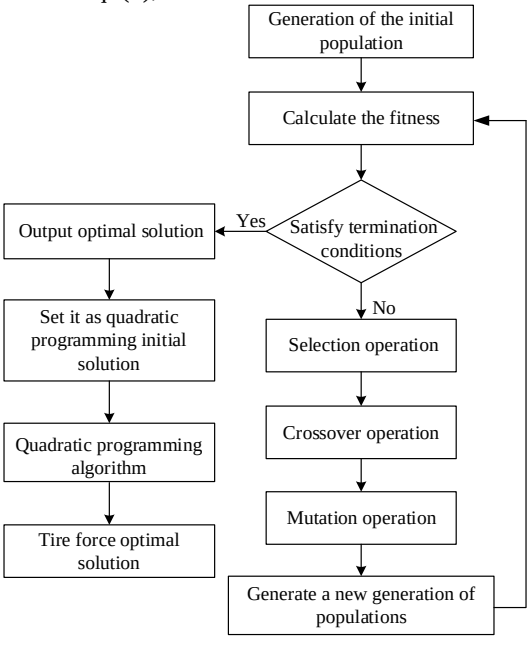


Figure 3. Flowchart of GA-QP algorithm.

https://doi.org/10.5194/ms-2026-196
Preprint. Discussion started: 19 November 2026
© Author(s) 2026. CC BY 4.0 License.



mechanical sciences DISCUSSIONS

2.3 Front wheel angle and wheel torque solution

The front wheel angle and longitudinal torque of each wheel are generated from the Dugoff tire inverse model and the wheel torque calculation formula, respectively. The Dugoff tire model is shown as follows.

$$\begin{cases} F_{xij} = C_{xij}\dfrac{s_{ij}}{1+s_{ij}} f(\lambda) \\ F_{yij} = C_{yij}\dfrac{\tan\alpha_{ij}}{1+s_{ij}} f(\lambda) \end{cases} \tag{13}$$

where $s_{ij}\,(i=f,r;j=l,r)$ is the slip ratio of each wheel, α_{ij} is side slip angle, C_{xij} is the longitudinal cornering stiffness of each wheel, C_{yij} is the lateral cornering stiffness of each wheel, $\lambda = \dfrac{\mu F_{zij}(1+s_{ij})}{2\sqrt{(C_{xij}s_{ij})^2+(C_{yij}\tan\alpha_{ij})^2}}$, $f(\lambda) = \begin{cases} (2-\lambda)\lambda, \lambda<1 \\ 1 \quad\quad ,\lambda\geq 1 \end{cases}$.

According to the above equation, the Dugoff tire inverse model can be deduced as follows.

$$\tan\alpha_{ij} = \frac{C_{xij}F_{yij}}{C_{yij}F_{xij}}s_{ij} \tag{14}$$

When $\lambda \geq 1$ holds, the following equation can be obtained by introducing Eq. (14) into Eq. (13).

$$\begin{cases} s_{ij} = \dfrac{F_{xij}}{C_{xij}-F_{xij}} \\ \alpha_{ij} = \arctan\dfrac{C_{xij}F_{yij}}{C_{yij}\left(C_{xij}-F_{xij}\right)} \end{cases} \tag{15}$$

When $\lambda < 1$ holds, the following equation can be obtained.

$$\begin{cases} s_{ij} = \dfrac{\mu^2 F_{xij}F_{zij}^2}{4C_{xij}\sqrt{F_{xij}^2+F_{yij}^2}\left(\mu F_z - \sqrt{F_{xij}^2+F_{yij}^2}\right)-\mu^2 F_{xij}F_{zij}^2} \\ \alpha_{ij} = \arctan\dfrac{C_{xij}\mu^2 F_{yij}F_{zij}^2}{4C_{xij}C_{yij}\sqrt{F_{xij}^2+F_{yij}^2}\left(\mu F_z - \sqrt{F_{xij}^2+F_{yij}^2}\right)-C_{yij}\mu^2 F_{xij}F_{zij}^2} \end{cases} \tag{16}$$

Based on the side slip angle in Eq. (16), the front wheel angle is derived as shown in the following equations.

$$\begin{cases} \delta_{fl} = \dfrac{v_y + a\omega_r}{v_x + B\omega_r/2} - \alpha_{fl} \\ \delta_{fr} = \dfrac{v_y + a\omega_r}{v_x - B\omega_r/2} - \alpha_{fr} \\ \delta_f = \dfrac{\delta_{fl}+\delta_{fr}}{2} \end{cases} \tag{17}$$

The wheel torque is calculated by following expression.

$$T_{xij} = F_{xij}R \tag{18}$$

where T_{xij} is the torque of each wheel, R is the rolling radius of the wheel.

https://doi.org/10.5194/ms-2026-196
Preprint. Discussion started: 19 November 2026
© Author(s) 2026. CC BY 4.0 License.



mechanical sciences DISCUSSIONS

3 GA-QP parameter adjustment strategy

In practice, the distribution parameters in the objective function of the GA-QP algorithm need to be adjusted in real time according to the stability of the vehicle. The phase plane method can directly reflect the stability state of the vehicle based on the relationship between the side slip angle and its derivative. Therefore, the parameters adjustment strategy of GA-QP algorithm based on phase plane method is proposed in this paper, so that the optimization results of tire force can be obtained under the various complex conditions.

3.1 Generation of stability boundary on the phase plane

The phase plane stability boundary is determined by the phase trajectory on the phase plane. If the trajectory line converges to the stable phase point (0,0), it can be concluded that the region is stable. It can be found that the stable region is bounded by the inner stable boundaries, the transitional region is the area between the inner and outer stable boundaries, and the unstable region is outside the outer stable boundary. The phase plane $\beta-\beta^{'}$ at the vehicle speed of 60 km/h is presented in Figure 4. under the condition of the road surface adhesion coefficient of 0.85. The stable boundaries of the phase plane $\beta-\beta^{'}$ are determined by Eq. (19) shown as follows.

$$\left|\beta^{'}+k\beta\right|=b_1 \tag{19}$$

where β is the side slip angle, k, b_1 are the boundary coefficients.

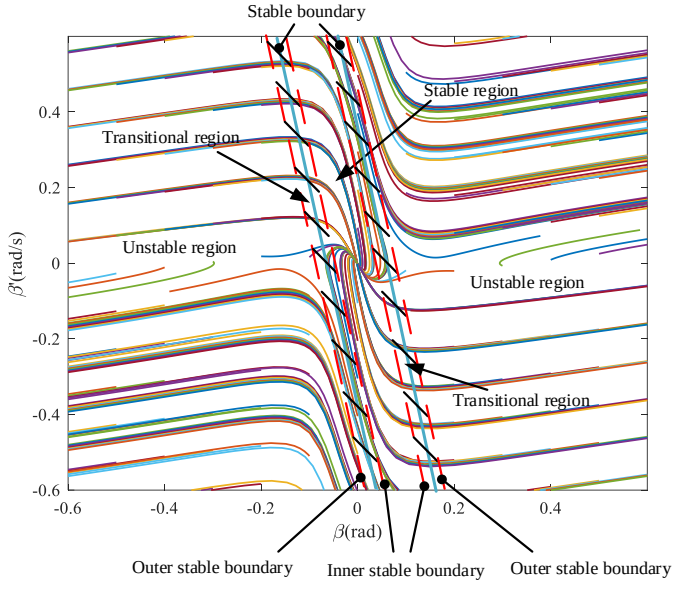


Figure 4. $\beta-\beta^{'}$ phase plane.

Since the stability boundary of phase plane is greatly influenced by the road surface adhesion coefficient, the boundary function of phase plane is fitted according to different adhesion coefficients. The coefficients of boundary function with respect to different adhesion coefficients are presented in Table 1.

https://doi.org/10.5194/ms-2026-196
Preprint. Discussion started: 19 November 2026
© Author(s) 2026. CC BY 4.0 License.



mechanical sciences DISCUSSIONS

Table 1. The coefficients of boundary function.

μ	k	b_1
0.2	1.60	0.08
0.3	2.30	0.10
0.4	2.85	0.12
0.5	3.69	0.16
0.6	4.01	0.25
0.7	4.55	0.30
0.8	5.07	0.32
0.9	5.52	0.37
1.0	5.86	0.40

It can be found in Table 1 that the correlation between the adhesion coefficients and the boundary coefficients is positive. The coefficients of boundary function are fitted as shown in Eq. (20) and Eq. (21).

$$k = -2.167\mu^2 + 7.933\mu + 0.1033 \tag{20}$$

$$b_1 = 0.04221\mu^2 + 0.3877\mu - 0.01729 \tag{21}$$

3.2 Parameters adjustment rules based on the phase plane

The formulas for calculating the distance on the phase plane are shown as follows.

$$\begin{cases} e_1 = \dfrac{\left|\beta^{'} + k\beta\right|}{\sqrt{1+k^2}} \\ e_0 = \dfrac{\left|2b_1\right|}{\sqrt{1+k^2}} \\ e_{\min} = 0.6e_0 \\ e_{\max} = 1.2e_0 \\ e_{\beta-\beta^{'}} = e_1 - e_{\min}/2 \end{cases} \tag{22}$$

where e_1 is the distance from the phase point to the middle line of the stable region on the phase plane, e_0 is the distance between the two stable boundaries on the phase plane, $e_{\min}$ is the distance between the two inner stable boundaries, $e_{\max}$ is the distance between the two outer stable boundaries, $e_{\beta-\beta^{'}}$ is the distance from the phase point to the inner stable boundary.

The longitudinal force distribution parameters of the front and rear wheels are obtained according to the position of phase point on the phase plane, and the corresponding parameters adjustment rules are shown as follows.

When $e_1 > \frac{1}{2}e_{\min}$ and $e_{\beta-\beta^{'}} / \frac{1}{2}e_{\max} \le 0.1$ or $e_1 \le \frac{1}{2}e_{\min}$ holds, $a_1 = 0.9$, $a_2 = 0.1$.

When $e_1 > \frac{1}{2}e_{\min}$ and $0.1 \le e_{\beta-\beta^{'}} / \frac{1}{2}e_{\max} \le 0.9$ holds, $a_1 = e_{\beta-\beta^{'}} / \frac{1}{2}e_{\max}$, $a_2 = 1 - a_1$.

When $e_1 > \frac{1}{2}e_{\min}$ and $e_{\beta-\beta^{'}} / \frac{1}{2}e_{\max} \ge 0.9$ holds, $a_1 = 0.1$, $a_2 = 0.9$.

https://doi.org/10.5194/ms-2026-196
Preprint. Discussion started: 19 November 2026
© Author(s) 2026. CC BY 4.0 License.



mechanical sciences DISCUSSIONS

4 Control strategy validation

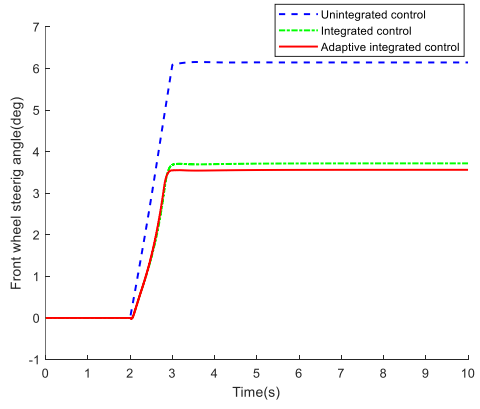
The chassis integrated control strategy of intelligent vehicle based on adaptive GA-QP algorithm is validated on the CarSim/Simulink joint simulation platform. The parameters of the vehicle are presented in Table 2. The simulations are carried out under the conditions of curved road with the adhesion coefficients of 0.85 and 0.25 respectively, at the speed of 70 km/h. Additionally, the adaptive integrated control strategy is compared with integrated control strategy and unintegrated control strategy.

Table 2. Vehicle parameters.

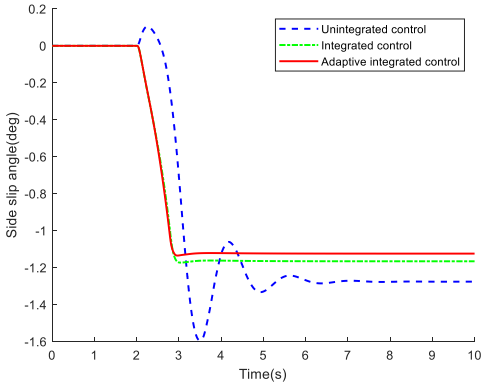
Parameters	Symbol/Unit	Value
Vehicle mass	m/ kg	1746
Distance from center of mass to front axle	a/ mm	1015
Distance from center of mass to rear axle	b/ mm	1895
The inertia of the vehicle around axis	I_z/ kg·m^2	1836
Front wheel lateral cornering stiffness	C_f / N·rad^{-1}	66900
Rear wheel lateral cornering stiffness	C_r / N·rad^{-1}	63700

4.1 High adhesion cornering condition

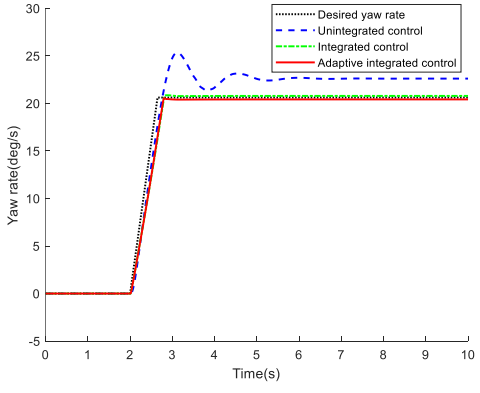
Under the cornering condition with the vehicle speed of 70 km/h and the adhesion coefficient of 0.85, the front wheel steering angle changes from 0 degree to 6 degrees in 1 second. In order to validate the proposed control strategy under the condition of medium-high speed and high adhesion, the simulation is carried out, and the results are shown in Figure 5.

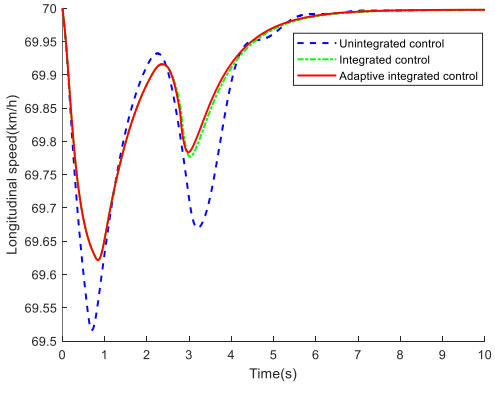


(a) Front wheel steering angle



(b) Side slip angle



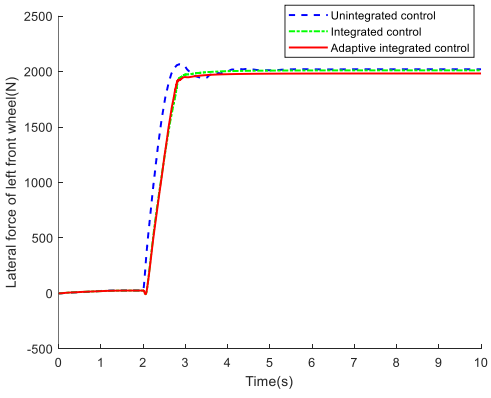


https://doi.org/10.5194/ms-2026-196
Preprint. Discussion started: 19 November 2026
© Author(s) 2026. CC BY 4.0 License.

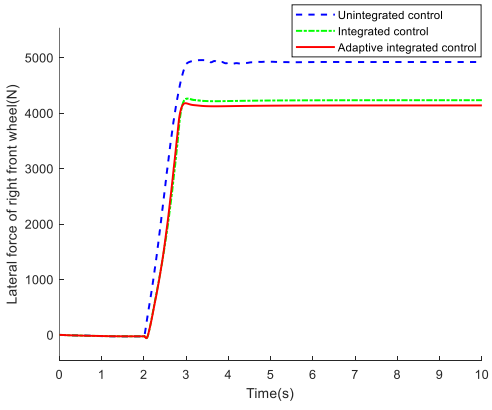


mechanical sciences DISCUSSIONS

(c) Yaw rate

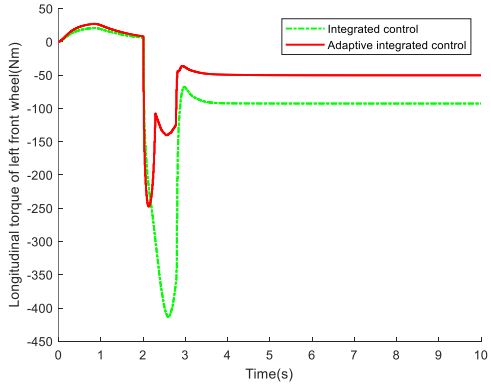


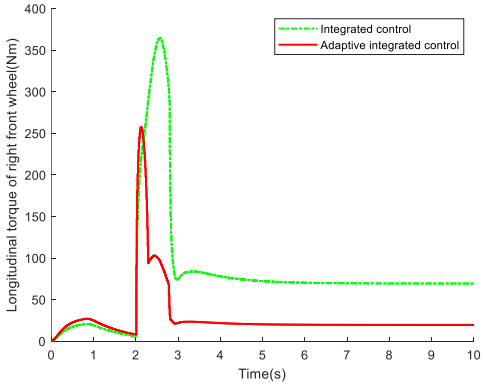
(d) Longitudinal speed



(e) Lateral force of left front wheel

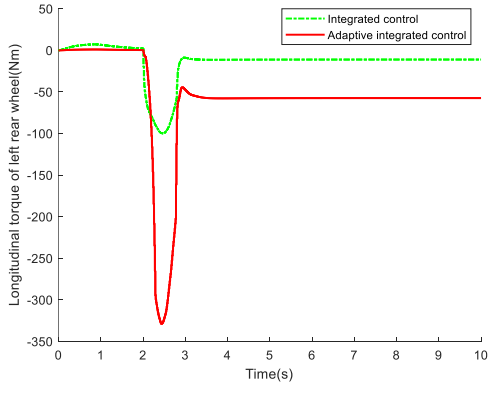
(f) Lateral force of right front wheel

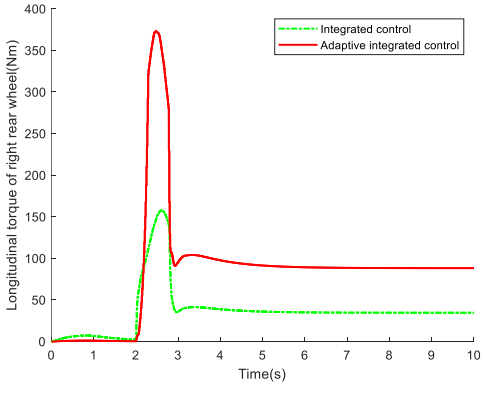




(g) Longitudinal torque of left front wheel

(h) Longitudinal torque of right front wheel





(i) Longitudinal torque of left rear wheel

(j) Longitudinal torque of right rear wheel

Figure 5. Simulation results on the curved road of high adhesion coefficient.

It can be seen from Figure 5(a) that the front wheel steering angle under unintegrated control strategy is significantly larger than that under adaptive integrated control strategy and integrated control strategy. However, the lateral force of left front wheel under the three control strategies is comparable, which indicates that the lateral force of left front wheel is saturated when the wheel angle reaches 3.5° as shown in Figure 5(e). The side slip angle continuously oscillates under

https://doi.org/10.5194/ms-2026-196
Preprint. Discussion started: 19 November 2026
© Author(s) 2026. CC BY 4.0 License.

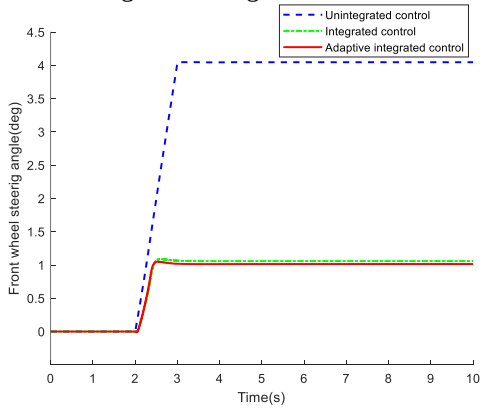


mechanical sciences DISCUSSIONS

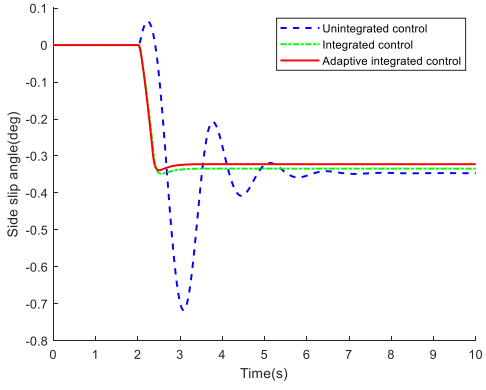
unintegrated control strategy, as shown in Figure 5(b). In contrast, under adaptive integrated control strategy, the side slip angle is decreased by 0.042° and 0.791° , respectively, in comparison to integrated control strategy and unintegrated control strategy, which indicates the improvement of handling stability of the vehicle. As can be seen in Figure 5(c), the yaw rate under the adaptive integrated control strategy and integrated control strategy is closer to the desired value than that under unintegrated control strategy. The longitudinal speed oscillation under the adaptive integrated control strategy and integrated control strategy is lower than that under the unintegrated control strategy, as illustrated in Figure 5(d). Figure 5(f) shows that the front wheel lateral force is significantly reduced under adaptive integrated control strategy and integrated control strategy compared to unintegrated control strategy. Figures 5(g), 5(h), 5(i), and 5(j) demonstrate that additional yaw moment is achieved by applying different torques to the left and right wheels, so as to regulate the yaw motion of the vehicle and improve the yaw stability. In addition, one can see from Figures 5(g), 5(h), 5(i), and 5(j) that the adaptive integrated control strategy distributes torque to the rear wheels more efficiently compared to integrated control strategy, which prevents front tire force saturation and improves driving safety.

4.2 Low adhesion cornering condition

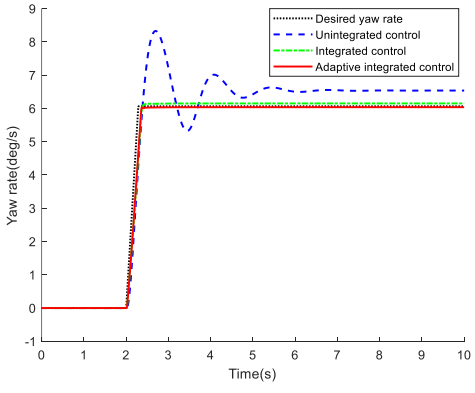
In order to further validate the proposed control strategy under the condition of low adhesion, the validation is carried out. In the simulation, the adhesion coefficient is set as 0.25, the vehicle speed is 70 km/h, and the front wheel steering angle changes from 0 degree to 4 degrees in 1 second. The simulation results are presented in Figure 6.



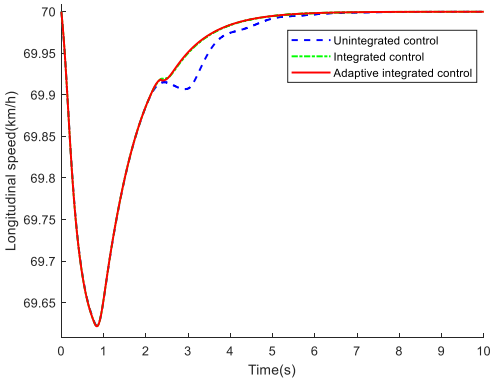
(a) Front wheel steering angle



(b) Side slip angle



(c) Yaw rate

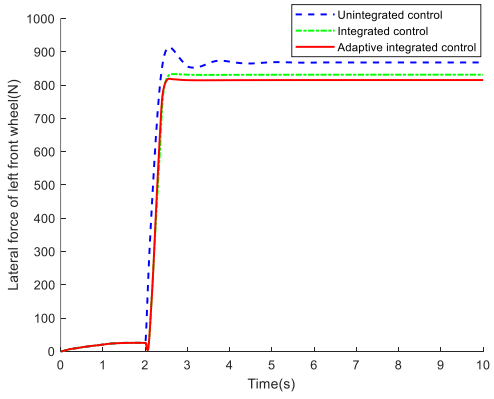


(d) Longitudinal speed

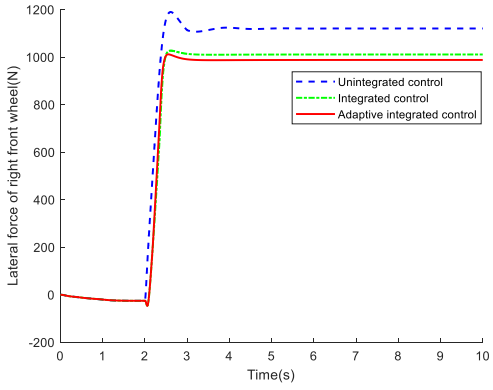
https://doi.org/10.5194/ms-2026-196
Preprint. Discussion started: 19 November 2026
© Author(s) 2026. CC BY 4.0 License.



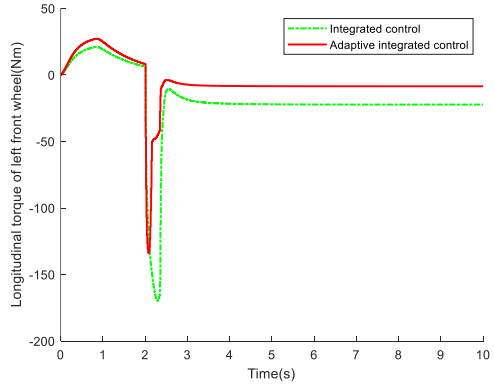
mechanical sciences
DISCUSSIONS



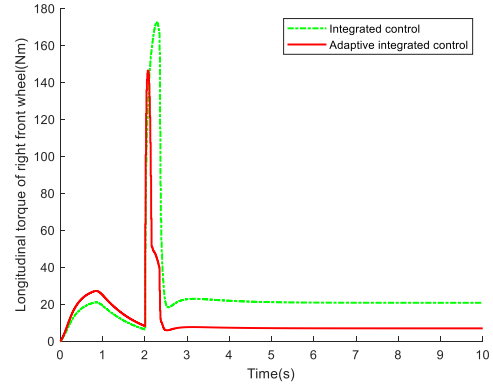
(e) Lateral force of left front wheel



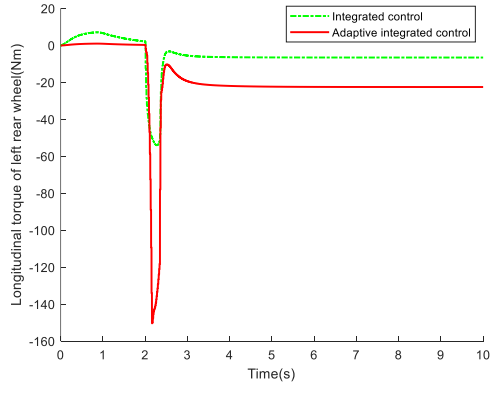
(f) Lateral force of right front wheel



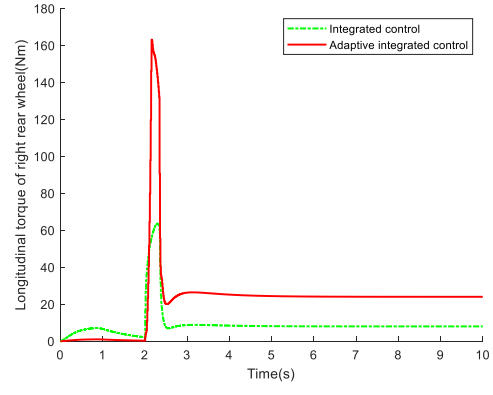
(g) Longitudinal torque of left front wheel



(h) Longitudinal torque of right front wheel



(i) Longitudinal torque of left rear wheel



(j) Longitudinal torque of right rear wheel

Figure 6. Simulation results on the curved road of low adhesion coefficient.

Under the condition of medium-high speed and low adhesion, as shown in Figure 6(b), the adaptive integrated control strategy respectively reduces the side slip angle by 0.017° and 0.393° compared to the integrated control strategy and unintegrated control strategy and eliminates the oscillations. Figure 6(c) shows that the yaw rate under the adaptive integrated control strategy and integrated control strategy is closer to the desired value than that under unintegrated control

https://doi.org/10.5194/ms-2026-196
Preprint. Discussion started: 19 November 2026
© Author(s) 2026. CC BY 4.0 License.



mechanical sciences
DISCUSSIONS

strategy, while the yaw rate under the unintegrated control strategy oscillates continuously between 2.5 seconds and 6 seconds. As illustrated in Figures 6(a), 6(e), and 6(f), although the steering angle is reduced from 4° to 1°, the lateral force of the left front wheel and the right front wheel under the adaptive integrated control strategy is only reduced by 52N and 133N respectively compared with the unintegrated control strategy, which indicates that the lateral force of the tire is close to saturation and the stability of the vehicle cannot be improved only by the control of the front wheels. Figures 6(g), 6(h), 6(i), and 6(j) show that the adaptive integrated control strategy distributes more wheel torque to the rear wheels compared with the integrated control strategy, which effectively reduces the load rate on the front wheels and improves the stability of vehicle.

5 Conclusion

To realize integrated control of the lateral and longitudinal force of intelligent vehicle under extreme working conditions, the chassis integrated control strategy based on adaptive GA-QP algorithm is proposed in this paper. The main conclusions of this paper are as follows:

By the adaptive GA-QP algorithm which combines the advantages of Genetic Algorithm (GA) and Quadratic Programming (QP) algorithm, the distribution of longitudinal and lateral force of tires is optimized and the dynamic performance of the vehicle is improved. Under the conditions of high adhesion coefficient and low adhesion coefficient, the adaptive integrated control strategy reduces the side slip angle and front wheel steering angle and maintains the yaw rate at the desired value, compared with the unintegrated control strategy.

The distribution parameters in the objective function of the GA-QP algorithm are dynamically adjusted based on the phase plane stability-judged principle. Compared with the integrated control strategy, the adaptive integrated control strategy reduces the longitudinal torque of the front wheel and increases the longitudinal torque of the rear wheel under the conditions of high and low adhesion, which effectively avoid the saturation of front wheel force and thus improve the stability of the vehicle.

This paper only focuses on the chassis integrated control of lateral and longitudinal force, and future research should refer to vertical control to further explore the integrated control strategy of the lateral, vertical and longitudinal force.

Code and data availability. The code and data included in this article can be made available by the corresponding author upon reasonable request. With respect to future applications, please note that the data and codes are confidential and cannot be made publicly available.

Author Contribution. Bin Tang and Yanjie Zhu designed research, performed research, analyzed data, and wrote the paper. Yanjie Zhu and Wei Mi collected and analyzed data. Haobing Jiang supervised this paper.

Financial support. This work was supported by the National Natural Science Foundation of China (Grant No. 52672512), Industry Prospect and Common Key Technologies Project in Zhenjiang City (Grant No. GY2024006), National Key Laboratory of Automotive Chassis Integration and Bionics (Grant No. 20230202).

Competing interests. The contact author has declared that none of the authors has any competing interests.

Disclaimer. Publisher's note: Copernicus Publications remains neutral with regard to jurisdictional claims in published maps and institutional affiliations.

References

Atindana, V. A., Xu, X., Kwaku, N. J., Akayeti, A., and Jiang, X.: A novel semi-active control of an integrated chassis and seat quasi-zero stiffness suspension system for off-road vehicles, J. Vib. Control, 30, 5536–5559, https://doi.org/10.1177/10775463231224835, 2024.

Chen, T., Chen, L., Xu, X., Cai, Y., Jiang, H., and Sun, X.: Passive fault-tolerant path following control of autonomous distributed drive electric vehicle considering steering system fault, Mech. Syst. Signal Process., 123, 298–315, https://doi.org/10.1016/j.ymssp.2019.01.019, 2019.

https://doi.org/10.5194/ms-2026-196
Preprint. Discussion started: 19 November 2026
© Author(s) 2026. CC BY 4.0 License.



mechanical sciences
DISCUSSIONS

Chen, X., Cheng, S., Li, S., Zhao, W., and Wang, C.: Lateral and longitudinal integrated emergency collision avoidance system with handling stability guarantee, IEEE Trans. Transp. Electrific., 10, 4930–4940, https://doi.org/10.1109/TTE.2023.3323643, 2024.

Cheng, S., Chen, H., Wang, Z., Yang, B., Lv, C., and Nakano, K.: A game theoretical chassis domain approach to trajectory tracking for automated vehicles, IEEE Trans. Veh. Technol., 72, 14051–14060, https://doi.org/10.1109/TVT.2023.3287687, 2023.

Choi, M. and Moon, C.: Development of coordinator for optimal tireforces distribution for vehicle dynamics control considering nonlinear tire characteristics, Int. J. Automot. Technol., 25, 689–698, https://doi.org/10.1007/s12239-024-00054-2, 2024.

Elhefnawy, A., Ragheb, H., Sharaf, A. M., and Hegazy, S.: On the control strategies for vehicle stability enhancement, Int. J. Heavy Veh. Syst., 27, 622–647, https://doi.org/10.1504/IJHVS.2020.111263, 2020.

Elhefnawy, A., Ragheb, H., Sharaf, A. M., and Hegazy, S.: Optimised coordinated chassis stability control using fuzzy genetic algorithm, Int. J. Heavy Veh. Syst., 27, 800–816, https://doi.org/10.1504/IJHVS.2020.112976, 2020.

Jiang, Y., Meng, H., Chen, G., Yang, C., Xu, X., Zhang, L., and Xu, H.: Differential-steering based path tracking control and energy-saving torque distribution strategy of 6WID unmanned ground vehicle, Energy, 254, 124209, https://doi.org/10.1016/j.energy.2022.124209, 2022.

Li, J., Luo, J., Guo, S., and Feng, B.: Research on yaw stability control strategy based on direct slip rate allocation, Electronics, 13, 193, https://doi.org/10.3390/electronics13010193, 2024.

Li, J., Wu, Z., Li, M., and Shang, Z.: Dynamic measurement method for steering wheel angle of autonomous agricultural vehicles, Agriculture, 14, 1602, https://doi.org/10.3390/agriculture14091602, 2024.

Liang, J., Lu, Y., Yin, G., Fang, Z., Zhuang, W., Ren, Y., Xu, L., and Li, Y.: A distributed integrated control architecture of AFS and DYC based on MAS for distributed drive electric vehicles, IEEE Trans. Veh. Technol., 70, 5565–5577, https://doi.org/10.1109/TVT.2021.3076105, 2021.

Lin, J., Zou, T., Su, L., Zhang, F., and Zhang, Y.: Optimal coordinated control of active front steering and direct yaw moment for distributed drive electric bus, Machines, 11, 640, https://doi.org/10.3390/machines11060640, 2023.

Liu, H., Yan, S., Shen, Y., Li, C., Zhang, Y., and Hussain, F.: Model predictive control system based on direct yaw moment control for 4WID self-steering agriculture vehicle, Int. J. Agric. Biol. Eng., 14, 175–181, https://doi.org/10.25165/j.ijabe.20211402.5283, 2021.

Liu, H., Liu, C., Han, L., and Xiang, C.: Handling and stability integrated control of AFS and DYC for distributed drive electric vehicles based on risk assessment and prediction, IEEE Trans. Intell. Transp. Syst., 23, 23148–23163, https://doi.org/10.1109/TITS.2022.3193891, 2022.

Liu, J., Liu, H., Wang, J., and Gu, H.: Coordinated lateral stability control of autonomous vehicles based on state estimation and path tracking, Machines, 11, 328, https://doi.org/10.3390/machines11030328, 2023.

Pérez-Villeda, H. M., Arechavaleta, G., and Morales-Díaz, A.: Multi-vehicle coordination based on hierarchical quadratic programming, Control Eng. Pract., 94, 104206, https://doi.org/10.1016/j.conengprac.2019.104206, 2020.

Scholtz, S. J. and Hamersma, H. A.: Investigating off-road vehicle lateral stability with integrated chassis control, Veh. Syst. Dyn., 62, 2974–2995, https://doi.org/10.1080/00423114.2024.2309894, 2024.

Song, Y., Shu, H., Chen, X., and Luo, S.: Direct-yaw-moment control of four-wheel-drive electrical vehicle based on lateral tyre–road forces and sideslip angle observer, IET Intell. Transp. Syst., 13, 303–312, https://doi.org/10.1049/iet-its.2018.5159, 2019.

Tang, C. and Khajepour, A.: Wheel modules with distributed controllers: a multi-agent approach to vehicular control, IEEE Trans. Veh. Technol., 69, 10879–10888, https://doi.org/10.1109/TVT.2020.3019376, 2020.

Vošahlík, D. and Haniš, T.: Traction control allocation employing vehicle motion feedback controller for four-wheel-independent-drive vehicle, IEEE Trans. Intell. Transp. Syst., 24, 14570–14579, https://doi.org/10.1109/TITS.2023.3295436, 2023.

Wang, C., He, R., Jing, Z., and Chen, S.: Coordinated path following control of 4WID-EV based on backstepping and model predictive control, Energies, 15, 5728, https://doi.org/10.3390/en15155728, 2022.

Wu, X., Zhou, B., Wu, T., and Pan, Q.: Research on intervention criterion and stability coordinated control of AFS and DYC, Int. J. Veh. Des., 90, 116–141, https://doi.org/10.1504/IJVD.2022.129163, 2022.

https://doi.org/10.5194/ms-2026-196
Preprint. Discussion started: 19 November 2026
© Author(s) 2026. CC BY 4.0 License.



mechanical sciences
DISCUSSIONS

Xiao, F., Hu, J., Jia, M., Zhu, P., and Deng, C.: A novel integrated control framework of AFS, ASS, and DYC based on ideal roll angle to improve vehicle stability, Adv. Eng. Inform., 54, 101764, https://doi.org/10.1016/j.aei.2022.101764, 2022.

Yang, Z., Lu, C., Sun, X., Ji, J., and Ding, Q.: Study on active disturbance rejection control of a bearingless induction motor based on an improved particle swarm optimization–genetic algorithm, IEEE Trans. Transp. Electrific., 7, 694–705, https://doi.org/10.1109/TTE.2020.3031338, 2021.

Zhang, N., Wang, J., Li, Z., Li, S., and Ding, H.: Multi-agent-based coordinated control of ABS and AFS for distributed drive electric vehicles, Energies, 15, 1919, https://doi.org/10.3390/en15051919, 2022.

Zhao, W., Yang, Z., and Wang, C.: Multi-objective optimization of chassis integrated system for electric wheel vehicle, Proc. Inst. Mech. Eng. C J. Mech. Eng. Sci., 233, 7–17, https://doi.org/10.1177/0954406218756444, 2019.

Zhu, S., Wang, B., Pan, S., Ye, Y., Wang, E., and Mao, H.: Task allocation of multi-machine collaborative operation for agricultural machinery based on the improved fireworks algorithm, Agronomy, 14, 710, https://doi.org/10.3390/agronomy14040710, 2024.

Zhu, Z., Tang, X., Qin, Y., Huang, Y., and Hashemi, E.: A survey of lateral stability criterion and control application for autonomous vehicles, IEEE Trans. Intell. Transp. Syst., 24, 10382–10399, https://doi.org/10.1109/TITS.2023.3280200, 2023.